Visual Servoing Based on Multirate Sampling Control
– Application of Perfect Disturbance Rejection Control –

Hiroshi Fujimoto   and   Yoichi Hori

Department of Electrical Engineering, The University of Tokyo
E-mail: fuji@hori.t.u-tokyo.ac.jp, hori@hori.t.u-tokyo.ac.jp

Abstract

In this paper, novel multirate controllers are proposed for digital control systems, where it is restricted that the sampling period of plant output is comparatively longer than the control period of plant input. The proposed controllers can assure perfect disturbance rejection at M intersample points in the steady state. Moreover, the novel scheme of repetitive control is proposed based on the open-loop estimation and switching function, which enables to reject periodical disturbance without any sacrifice of the feedback characteristics. The proposed methods are applied to the visual servo system, and the advantages of these approaches are demonstrated by simulations.

1 Introduction

A digital control system usually has two samplers $\mathcal{S}$ for the reference signal $r(t)$ and the output $y(t)$, and one holder $\mathcal{H}$ of the input $u(t)$, as shown in Fig. 1. Therefore, there exist three time periods T_r, T_y, and T_u which represent the period of $r(t), y(t)$, and $u(t)$, respectively. The input period T_u is generally decided by the speed of the actuator, D/A converter, or the calculation on the CPU. On the other hand, the output period T_y is also determined by the speed of the sensor or the A/D converter. Practical control systems usually hold the restrictions on T_u and/or T_y. Thus, the conventional digital control systems make these three periods equal to the longer period between T_u and T_y.

In this paper, the digital control systems with longer sampling period $(T_u < T_y)$ are considered. This restriction may be general because D/A converters are usually faster than the A/D converters. The first example which has this restriction is the visual servo system of robot manipulator [1, 2]. Although the sampling period of the vision sensor such as a CCD camera is comparatively slow (over 33 [ms]), the control
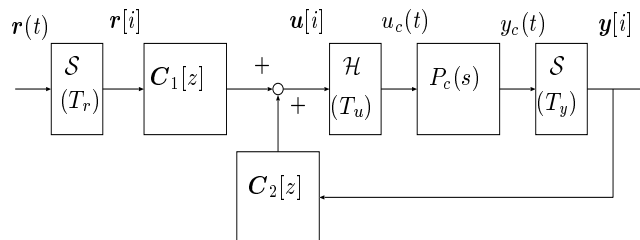

Figure 1: Two-degree-of-freedom control system.

period of joint servo is fast (under 1 [ms]). Therefore, the multirate controllers have been developed and implemented to the visual servo system [3, 4, 5].

The second example is the head positioning system of hard disk drives, in which the head position is detected by the discrete servo signal. Thus, the sampling frequency is restricted because it is determined by the rotation frequency and number of the servo signals. On the other hand, the control frequency of the actuator (voice coil motor) can be set faster than the sampling frequency of the head position. Therefore, the multirate estimation and control have been applied to hard disk drives in [6].

The third example is the velocity or position control of industrial motors with low precision encoder. In these systems, the sampling period cannot be set so fast, because the velocity information is not able to be detected precisely in the low speed region. Therefore, [7] has developed the instantaneous speed observer, which estimates the intersample velocity in use of the discrete-time observer.

For these systems with longer sampling periods, it is difficult to reject disturbance in high frequency region because the Nyquist frequency is relatively low. In this paper, multirate sampling control is introduced, in which the control input is changed N times during one sampling period. Using this scheme, novel multirate feedback controllers are proposed, which achieve disturbance rejection even in the semi-Nyquist frequency region. Moreover, the proposed methods are applied to the visual servo system of robot manipulator. In [6],
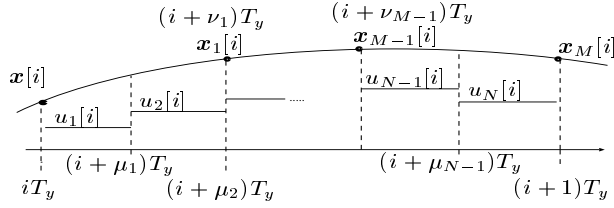
Figure 2: Multirate sampling control.

a novel multirate feedforward controller is proposed which assures the perfect tracking at M intersample points. Thus, this paper deals with only the feedback controller.

In the repetitive control system [8], conventional single-rate controllers do not have enough intersample performance to reject disturbance in the semi-Nyquist frequency region [9]. On the other hand, authors proposed a novel multirate feedback controller, which achieves the perfect disturbance rejection at M intersample points [6]. In this paper, the proposed approach is modified to be applicable to the visual servo system, in which the target object moves fast and periodically.

Repetitive feedback controllers based on the internal model principle have disadvantages that the closed-loop characteristics become worse and difficult to assure stability robustness [10]. Therefore, this paper proposes novel approach which never has these problems, based on the open-loop estimation with switching function and disturbance rejection by feedforward approach.

2 Design of the multirate feedback controller

In this section, the multirate feedback controller is proposed, which guarantees the perfect disturbance rejection at M intersample points at the steady state.

In the proposed multirate scheme, the plant input is changed N times during T_y and the plant state is evaluated M times in this interval, as shown in Fig. 2. The positive integers M and N are referred to as input and state multiplicities, respectively. N is determined by the hardware restriction. In this paper, the state multiplicity is defined as $M = N/n$, where n is the plant order.

In Fig. 2, $\mu_j (j = 0, 1, \cdots, N)$ and $\nu_k (k = 1, \cdots, M)$ are the parameters for the timing of the input changing and the state evaluation, which satisfy the conditions (1) and (2).

$$0 = \mu_0 < \mu_1 < \mu_2 < ... < \mu_N = 1 \qquad (1)$$

$$0 < \nu_1 < \nu_2 < ... < \nu_M = 1 \qquad (2)$$

If T_y is divided at same intervals, the parameters are set to $\mu_j = j/N, \nu_k = k/M$.

For simplification, the continuous-time plant is assumed to be SISO system in this paper. The proposed methods, however, can be extended to deal with the MIMO system by the same way as [11].

2.1 Plant discretization by multirate sampling

Consider the continuous-time plant described by

$$\dot{\boldsymbol{x}}(t) = \boldsymbol{A_c}\boldsymbol{x}(t) + \boldsymbol{b_c}u(t) , \quad y(t) = \boldsymbol{c_c}\boldsymbol{x}(t). \qquad (3)$$

The discrete-time plant discretized by the multirate sampling control of Fig. 2 becomes

$$\boldsymbol{x}[i+1] = \boldsymbol{A}\boldsymbol{x}[i] + \boldsymbol{B}\boldsymbol{u}[i] , \quad y[i] = \boldsymbol{C}\boldsymbol{x}[i], \qquad (4)$$

where $\boldsymbol{x}[i] = \boldsymbol{x}(iT_y)$, and matrices $\boldsymbol{A}, \boldsymbol{B}, \boldsymbol{C}$ and vectors $\boldsymbol{u}$ are given by

$$\left[\begin{array}{c|c} \boldsymbol{A} & \boldsymbol{B} \\ \hline \boldsymbol{C} & \boldsymbol{O} \end{array} \right] := \left[\begin{array}{c|ccc} e^{\boldsymbol{A_c}T_y} & \boldsymbol{b}_1 & \cdots & \boldsymbol{b}_N \\ \hline \boldsymbol{c_c} & 0 & \cdots & 0 \end{array} \right] , \qquad (5)$$

$$\boldsymbol{b}_j := \int_{(1-\mu_j)T_y}^{(1-\mu_{(j-1)})T_y} e^{\boldsymbol{A_c}\tau} \boldsymbol{b_c} d\tau , \quad \boldsymbol{u} := [u_1, \cdots, u_N]^T,$$

where $u_j[i]$ is the control input for $(i + \mu_{j-1})T_y \leq t < (i + \mu_j)T_y$ $(j = 1, \cdots, N)$. The intersample plant state at $t = (i + \nu_k)T_y$ is represented by

$$\tilde{\boldsymbol{x}}[i] = \tilde{\boldsymbol{A}}\boldsymbol{x}[i] + \tilde{\boldsymbol{B}}\boldsymbol{u}[i], \qquad (6)$$

where $\tilde{\boldsymbol{x}}[i]$ is a vector composed of the intersample plant state $\boldsymbol{x}_k[i] := \boldsymbol{x}((i + \nu_k)T_y)$ of Fig. 2.

$$\begin{aligned} \tilde{\boldsymbol{x}}[i] &:= [\boldsymbol{x}_1^T[i], \cdots, \boldsymbol{x}_M^T[i]]^T \\ &= [\boldsymbol{x}_1^T((i + \nu_1)T_y), \cdots, \boldsymbol{x}_M^T((i + 1)T_y)]^T \quad (7) \end{aligned}$$

The coefficient matrices of (6) are given by

$$[\ \tilde{\boldsymbol{A}} \ | \ \tilde{\boldsymbol{B}} \ ] := \left[\begin{array}{c|ccc} \tilde{\boldsymbol{A}}_1 & \tilde{\boldsymbol{b}}_{11} & \cdots & \tilde{\boldsymbol{b}}_{1N} \\ \vdots & \vdots & & \vdots \\ \tilde{\boldsymbol{A}}_M & \tilde{\boldsymbol{b}}_{M1} & \cdots & \tilde{\boldsymbol{b}}_{MN} \end{array} \right],$$

$$\tilde{\boldsymbol{A}}_k := e^{\boldsymbol{A_c}\nu_k T_y},$$

$$\tilde{\boldsymbol{b}}_{kj} := \left\{ \begin{array}{ll} \mu_j < \nu_k : & \int_{(\nu_k - \mu_j)T_y}^{(\nu_k - \mu_{(j-1)})T_y} e^{\boldsymbol{A_c}\tau} \boldsymbol{b_c} d\tau \\ \mu_{(j-1)} < \nu_k \leq \mu_j : & \int_0^{(\nu_k - \mu_{(j-1)})T_y} e^{\boldsymbol{A_c}\tau} \boldsymbol{b_c} d\tau \\ \nu_k \leq \mu_{(j-1)} : & 0 \end{array} \right. .$$
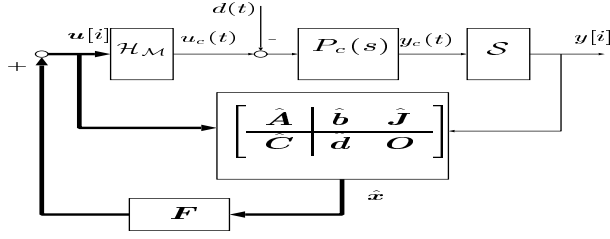
Figure 3: Multirate control with disturbance observer.

2.2 Design of the perfect disturbance rejection controller

In this section, the perfect disturbance rejection controller is proposed based on the state space design of the disturbance observer.

Consider the continuous-time plant model described by

$$\dot{\boldsymbol{x}}_p(t) = \boldsymbol{A}_{cp}\boldsymbol{x}_p(t) + \boldsymbol{b}_{cp}(u(t) - d(t)) \qquad (8)$$

$$y(t) = \boldsymbol{c}_{cp}\boldsymbol{x}_p(t), \qquad (9)$$

where $d(t)$ is the disturbance input. Let the disturbance model be

$$\dot{\boldsymbol{x}}_d(t) = \boldsymbol{A}_{cd}\boldsymbol{x}_d(t) , \ d(t) = \boldsymbol{c}_{cd}\boldsymbol{x}_d(t). \qquad (10)$$

For example, the step type disturbance is modeled by $\boldsymbol{A}_{cd} = 0, \boldsymbol{c}_{cd} = 1$, and the sinusoidal type disturbance with frequency ω_d is also modeled by

$$\boldsymbol{A}_{cd} = \begin{bmatrix} 0 & 1 \\ -\omega_d^2 & 0 \end{bmatrix}, \quad \boldsymbol{c}_{cd} = [1, 0]. \qquad (11)$$

The continuous-time augmented system consisting of (8) and (10) is represented by

$$\dot{\boldsymbol{x}}(t) = \boldsymbol{A}_c\boldsymbol{x}(t) + \boldsymbol{b}_c u(t) \qquad (12)$$

$$y(t) = \boldsymbol{c}_c\boldsymbol{x}(t) \qquad (13)$$

$$\boldsymbol{A}_c := \begin{bmatrix} \boldsymbol{A}_{cp} & -\boldsymbol{b}_{cp}\boldsymbol{c}_{cd} \\ \boldsymbol{O} & \boldsymbol{A}_{cd} \end{bmatrix}, \boldsymbol{b}_c := \begin{bmatrix} \boldsymbol{b}_{cp} \\ \boldsymbol{0} \end{bmatrix}, \boldsymbol{x} := \begin{bmatrix} \boldsymbol{x}_p \\ \boldsymbol{x}_d \end{bmatrix}$$

$$\boldsymbol{c}_c := [\boldsymbol{c}_{cp}, \boldsymbol{0}].$$

Discretizing (12) with the multirate hold $\mathcal{H}_\mathcal{M}$, the intersample plant state at $t = (i + \nu_k)T_y$ can be calculated from the kth row of (6) by

$$\boldsymbol{x}[i + \nu_k] = \tilde{\boldsymbol{A}}_k\boldsymbol{x}[i] + \tilde{\boldsymbol{B}}_k\boldsymbol{u}[i] \qquad (14)$$

$$\tilde{\boldsymbol{A}}_k = \begin{bmatrix} \tilde{\boldsymbol{A}}_{pk} & \tilde{\boldsymbol{A}}_{pdk} \\ \boldsymbol{O} & \tilde{\boldsymbol{A}}_{dk} \end{bmatrix}, \tilde{\boldsymbol{B}}_k = \begin{bmatrix} \tilde{\boldsymbol{B}}_{pk} \\ \boldsymbol{O} \end{bmatrix}.$$

For the plant (12) discretized by (4), the discrete-time observer on the sampling points is obtained from the Gopinath's method by

$$\hat{\boldsymbol{v}}[i + 1] = \hat{\boldsymbol{A}}\hat{\boldsymbol{v}}[i] + \hat{\boldsymbol{b}}y[i] + \hat{\boldsymbol{J}}\boldsymbol{u}[i] \qquad (15)$$

$$\hat{\boldsymbol{x}}[i] = \hat{\boldsymbol{C}}\hat{\boldsymbol{v}}[i] + \hat{\boldsymbol{d}}y[i]. \qquad (16)$$

As shown in Fig. 3, let the feedback control law be

$$\boldsymbol{u}[i] = \boldsymbol{F}_p\hat{\boldsymbol{x}}_p[i] + \boldsymbol{F}_d\hat{\boldsymbol{x}}_d[i] = \boldsymbol{F}\hat{\boldsymbol{x}}[i], \qquad (17)$$

where $\boldsymbol{F} := [\boldsymbol{F}_p, \boldsymbol{F}_d]$. Letting $\boldsymbol{e}_v$ be the estimation errors of the observer ($\boldsymbol{e}_v = \hat{\boldsymbol{v}} - \boldsymbol{v}$), the following equation is obtained.

$$\hat{\boldsymbol{x}}[i] = \boldsymbol{x}[i] + \hat{\boldsymbol{C}}\boldsymbol{e}_v[i]. \qquad (18)$$

From (14) to (18), the closed-loop system is represented by

$$\begin{bmatrix} \boldsymbol{x}_p[i + \nu_k] \\ \boldsymbol{x}_d[i + \nu_k] \\ \boldsymbol{e}_v[i + 1] \end{bmatrix} =$$

$$\begin{bmatrix} \tilde{\boldsymbol{A}}_{pk} + \tilde{\boldsymbol{B}}_{pk}\boldsymbol{F}_p & \tilde{\boldsymbol{A}}_{pdk} + \tilde{\boldsymbol{B}}_{pk}\boldsymbol{F}_d & \tilde{\boldsymbol{B}}_{pk}\boldsymbol{F}\hat{\boldsymbol{C}} \\ \boldsymbol{O} & \tilde{\boldsymbol{A}}_{dk} & \boldsymbol{O} \\ \boldsymbol{O} & \boldsymbol{O} & \hat{\boldsymbol{A}} \end{bmatrix} \begin{bmatrix} \boldsymbol{x}_p[i] \\ \boldsymbol{x}_d[i] \\ \boldsymbol{e}_v[i] \end{bmatrix}.$$

Because full row rank of the matrix $\tilde{\boldsymbol{B}}_{pk}$ can be assured [12], $\boldsymbol{F}_d$ can be selected so as to the (1,2) element of the above equation becomes zero for all $k = 1, \cdots, M$.

$$\tilde{\boldsymbol{A}}_{pdk} + \tilde{\boldsymbol{B}}_{pk}\boldsymbol{F}_d = \boldsymbol{O} \qquad (19)$$

The simultaneous equation of (19) for all k becomes

$$\tilde{\boldsymbol{A}}_{pd} + \tilde{\boldsymbol{B}}_p\boldsymbol{F}_d = \boldsymbol{O}, \qquad (20)$$

$$[\ \tilde{\boldsymbol{A}}_{pd}\ |\ \tilde{\boldsymbol{B}}_p\ ] := \begin{bmatrix} \tilde{\boldsymbol{A}}_{pd1} & \tilde{\boldsymbol{B}}_{p1} \\ \vdots & \vdots \\ \tilde{\boldsymbol{A}}_{pdM} & \tilde{\boldsymbol{B}}_{pM} \end{bmatrix}. \qquad (21)$$

From (20), $\boldsymbol{F}_d$ is obtained by

$$\boldsymbol{F}_d = -\tilde{\boldsymbol{B}}_p^{-1}\tilde{\boldsymbol{A}}_{pd}. \qquad (22)$$

By (19), the influence from disturbance $\boldsymbol{x}_d[i]$ to the intersample state $\boldsymbol{x}_p[i + \nu_k]$ at $t = (i + \nu_k)T_y$ can become zero. Moreover, $\boldsymbol{x}_p[i]$ and $\boldsymbol{e}_v[i]$ on the sampling point converge to zero at the rate of the eigenvalues of $\tilde{\boldsymbol{A}}_{pM} + \tilde{\boldsymbol{B}}_{pM}\boldsymbol{F}_p$ and $\hat{\boldsymbol{A}}$ (the poles of the regulator and observer). Therefore, the perfect disturbance rejection is achieved ($\boldsymbol{x}_p[i + \nu_k] = 0$) in the steady state. The poles of the regulator and observer should be tuned by the tradeoff between the performance and stability robustness.

Substituting (15) for (17), the feedback type controller is obtained by

$$\begin{bmatrix} \hat{\boldsymbol{v}}[i + 1] \\ \boldsymbol{u}[i] \end{bmatrix} = \begin{bmatrix} \hat{\boldsymbol{A}} + \hat{\boldsymbol{J}}\boldsymbol{F}\hat{\boldsymbol{C}} & \hat{\boldsymbol{b}} + \hat{\boldsymbol{J}}\boldsymbol{F}\hat{\boldsymbol{d}} \\ \boldsymbol{F}\hat{\boldsymbol{C}} & \boldsymbol{F}\hat{\boldsymbol{d}} \end{bmatrix} \begin{bmatrix} \hat{\boldsymbol{v}}[i] \\ y[i] \end{bmatrix}. \qquad (23)$$
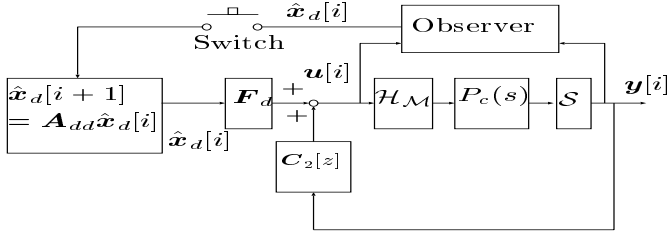
Figure 4: Feedforward repetitive control.

3 Repetitive control based on multirate control

In this section, two multirate repetitive controllers are proposed, which are 1) feedback approach based on internal model principle and 2) feedforward disturbance rejection approach based on the open-loop estimation and switching function.

3.1 Feedback repetitive control

The periodic disturbance of $T_0 := 2\pi/\omega_0$ is represented by

$$d(t) = a_0 + \sum_{k=1}^{\infty} a_k \cos k\omega_0 t + b_k \sin k\omega_0 t, \qquad (24)$$

where ω_0 is known, a_k and b_k are unknown parameters. Letting the disturbance model (10) be (24), the repetitive feedback controller is obtained by (23), which has internal model $s^2 + (k\omega_0)^2$ in discrete-time domain. Moreover, the repetitive disturbance is perfectly rejected ($x_p[i + \nu_k] = 0$) at M intersample points in the steady state.

3.2 Feedforward repetitive control

The repetitive feedback control based on the internal model principle has disadvantages that the closed-loop characteristics become worse and difficult to assure stability robustness [10]. Therefore, in this section, novel repetitive controller based on the open-loop estimation and feedforward disturbance rejection is proposed, as shown in Fig. 4.

The repetitive disturbance is estimated by the open-loop disturbance observer. When the estimation converges to the steady state, the switch turns on at $t = t_0$. After that, the switch turns off immediately. The repetitive disturbance is calculated by (25) from the initial value $\hat{x}_d[t_0]$ which has the amplitude and phase information of the disturbance.

$$\hat{x}_d[i + 1] = \boldsymbol{A}_{dd}\hat{x}_d[i], \boldsymbol{A}_{dd} = e^{\boldsymbol{A}_{cd}T_y} \qquad (25)$$

Because the feedforward gain $\boldsymbol{F}_d$ is obtained by (22), the perfect disturbance rejection is achieved at M in-
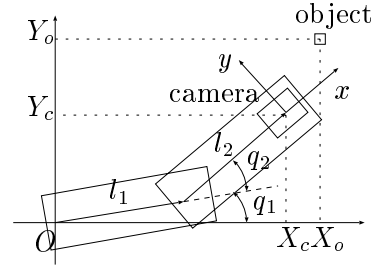
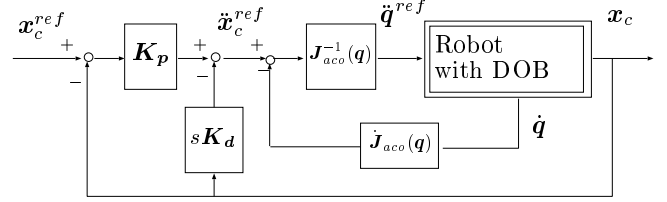

Figure 5: Two-link DD robot with camera.

Figure 6: Workspace controller (inner-loop).

tersample points. The advantage of this approach is that the stability robustness can be guaranteed easily only by the conventional feedback controller $\boldsymbol{C}_2[z]$ which does not have the internal model.

4 Applications to visual servo system

In this section, the visual servo problem is considered, in which the camera mounted on the robot manipulator is controlled to track the moving object, as shown in Fig. 5. It is assumed that the motion of the object is periodic, and repetitive disturbance rejection control is applied, which was developed in section 3.

Because the sampling period of the camera is longer than the control period of the joint servo, the proposed approach is applicable. In order to focus on the dynamical problems of the multirate system, the kinematical problems of the visual servo system are assumed to be simple; the object movement is in two-dimensional plane, and the depth information between the camera and the object z is known.

4.1 Modeling of visual servo system

First, the workspace position controller is designed in order to control camera position, as shown in Fig. 6 [13]. Because this controller employs the robust disturbance observer (DOB) in the joint space, each joint axis is decoupled. Therefore, if the non-singularity of the Jacobian $\boldsymbol{J}_{aco}$ is assured, the transfer function from the work space acceleration command $\ddot{\boldsymbol{x}}_c^{ref}$ to the work space position $\boldsymbol{x}_c(= [X_c, Y_c]^T)$ can be regarded
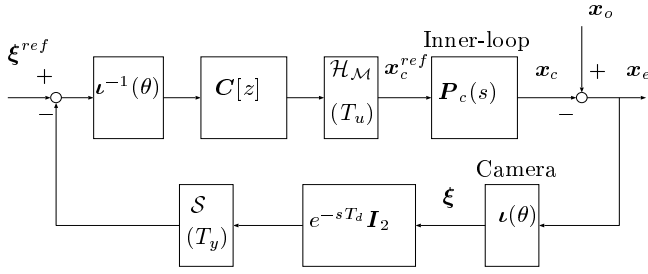
Figure 7: Visual servo system.

(a) Feedback   (b) Feedforward

Figure 8: Frequency responses $S[z]$ and $T[z]$.

as a double integrator system in the frequency region under the cut-off frequency [13]. Letting $\boldsymbol{x}_c^{ref}$ be the control input $\boldsymbol{u}$ of the outer visual servo system, the plant is modeled by the analog system (26) because the sampling period of the inter-loop is very short (under 1 [ms]).

$$\boldsymbol{x}_c(s) = \boldsymbol{P}_c(s)\boldsymbol{u}(s), \quad \boldsymbol{P}_c(s) := \frac{K_p}{s^2 + K_d s + K_p}\boldsymbol{I}_2 \quad (26)$$

In Fig. 6, the parameters of the position controller are set to $\boldsymbol{K}_p = diag\{900, 900\}$ and $\boldsymbol{K}_d = diag\{60, 60\}$.

Next, the perspective model of the camera is derived. In Fig. 6, the object position (x, y) on the camera coordinate system is determined only by the relative position between the camera position $\boldsymbol{x}_c$ and object position $\boldsymbol{x}_o$. Therefore, the following model is obtained because the (x, y) is mapped to the feature point $\boldsymbol{\xi}$ on the image plane [3].

$$\boldsymbol{\xi} = \frac{f}{z}\left[\begin{array}{c} x \\ y \end{array}\right] = \frac{f}{z}\left[\begin{array}{cc} \cos\theta & \sin\theta \\ -\sin\theta & \cos\theta \end{array}\right]\left[\begin{array}{c} X_o - X_c \\ Y_o - Y_c \end{array}\right]$$
$$(27)$$

Here f is the focus distance, z is the distance between the object and camera in $Z-$axis direction, and $\theta := q_1 + q_2$. (27) is defined by $\boldsymbol{\xi} = \iota(\theta)(\boldsymbol{x}_o - \boldsymbol{x}_c) = \iota(\theta)\boldsymbol{x}_e$.

Fig. 7 shows the proposed control system. In this paper, the desired feature $\boldsymbol{\xi}^{ref}$ is set to zero because the camera is controlled to be positioned just below the object. The movement of the object can be modeled as the output disturbance $\boldsymbol{x}_o$. Therefore, the proposed method can achieve high performance tracking because the periodic motion can be rejected by the proposed method. Moreover, the control system of Fig. 7 is linearized and diagonalized by the inverse transformation $\iota^{-1}(\theta)$ of (27)[1]. Thus, the controllers can be designed independently in the x and y axes. The sampling period of the image and the control period of the position command $\boldsymbol{x}_c^{ref}$ are set to 40 [ms] and 10 [ms], respectively. Because the input multiplicity is

---

[1] In case of the setup of Fig. 7, $\iota^{-1}(\theta)$ is easily obtained from the inverse matrix of (27). In general case, it can be calculated from the inverse Jacobian [2].
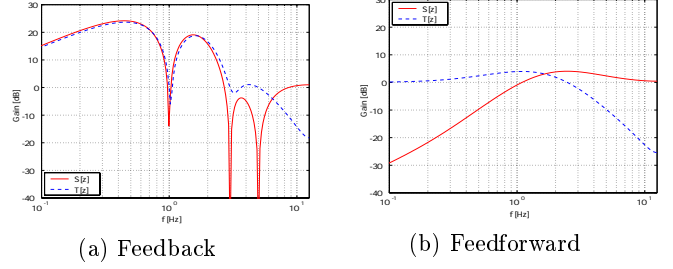

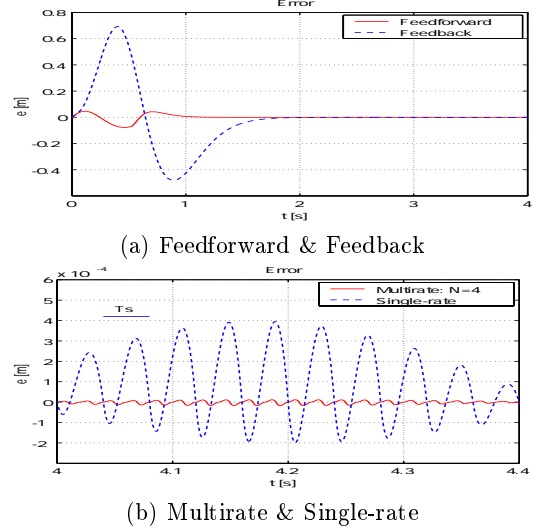(a) Feedforward & Feedback

(b) Multirate & Single-rate

Figure 9: Position error $X_o - X_c$.

$N = 4$ and the order of plant (26) is $n = 2$, perfect disturbance rejection is assured at $2(= N/n)$ intersample points. The T_d represents the time delay caused by the image processing. This delay generates the difficulty in control system. However, the proposed multirate sampling control is applicable to the system with time delay [14].

4.2 Simulation results

The repetitive disturbance is modeled on the $k = 1, 3, 5$ order[2]. The period of the object movement is $T_0 = 1[s]$.

Fig. 8 shows the sensitivity and complementary sensitivity functions $S[z]$ and $T[z]$ both of the feedback (Fig. 3) and the feedforward (Fig. 4) approaches. Fig. 8(a) indicates the disadvantages of the feedback repetitive controller, where the closed-loop characteristics become worse and difficult to assure stability robustness. On the other hand, in the proposed feedforward repetitive control (Fig. 4), the closed-loop characteris-

---

[2] These modes should be selected from the experimental analysis of the target motion.
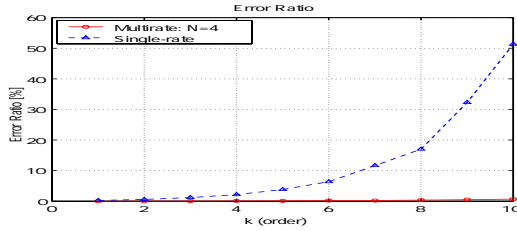
Figure 10: Error ratio $E_R(k)$.

tics depend only on $C_2[z]$ which does not need to have the internal model of repetitive disturbance. Therefore, the feedback characteristics are better than the feedback approach as shown in Fig. 8(b).

Fig. 9 shows the simulated results of position errors $X_o - X_c$ under the circular movement of the object. As shown in Fig. 9(a), the position error of the feedforward controller converges quickly after the switching action at $t_0 = 0.5[s]$, while that of the feedback controller has large transient error. In the steady state, the errors of the plant position and velocity become zero at every $T_y/2$ by the proposed controller, as shown in Fig. 9(b). The intersample position error of the proposed multirate method is much smaller than that of the single-rate controller.

Fig. 10 shows analyzed results of the error ratio $E_R(k)$ for the disturbance order k. Considering the intersample response, the error ratio is calculated by

$$E_R^2(k) := \frac{\int_{t_s}^{t_s + kT_0} (X_o(t) - X_c(t))^2 \, dt}{\int_{t_s}^{t_s + kT_0} X_o^2(t) dt}, \qquad (28)$$

where $X_o(t) = \sin k\omega_0 t, \omega_0 = 2\pi/T_0$, and t_s is selected as 2 [s] in order to evaluate the steady state. In the high frequency region close to the Nyquist frequency, the disturbance rejection performance is much improved by the proposed multirate control, compared with the single-rate controller. Therefore, it is found that the proposed method can demonstrate much effective performance for high-order disturbance.

5 Conclusion

In this paper, the repetitive disturbance rejection controllers were applied to the visual servo system of robot manipulator based on the multirate sampling control. Because the proposed control system assured the perfect disturbance rejection at M intersample points, the control system has achieved high tracking performance. Next, the novel scheme of repetitive control was proposed based on the open-loop estimation

and switching function, which enabled to reject periodical disturbance without any sacrifice of the feedback characteristics. The experimental results of the proposed method will be presented in the next opportunity.

References

[1]   L. E. Weiss, A. C. Sanderson, and C. P. Newman, "Dynamic sensor based control of robots with visual feedback," *IEEE J. Robotics and Automation*, vol. 3, no. 5, pp. 404–417, 1987.

[2]   S. Hutchinson, G. D. Hager, and P. I. Corke, "A tutorial on visual servo control," *IEEE Trans. Robotics and Automation*, vol. 12, no. 5, pp. 3745–3750, 1996.

[3]   K. Hashimoto and H. Kimura, "Visual servoing with nonlinear observer," *IEEE Int. Conf. Robotics and Automation*, pp. 484–489, 1995.

[4]   M. Nemani, T. C. Tsao, and S. Hutchinson, "Multi-rate analysis and design of visual feedback digital servo-control system," *ASME, J. Dynam. Syst., Measur., and Contr.*, vol. 116, pp. 44–55, March 1994.

[5]   J. T. Feeddma and O. R. Mitchell, "Vision guided servoing with feature-based trajectory generation," *IEEE Trans. Robotics and Automation*, vol. 5, no. 5, pp. 691–700, 1989.

[6]   H. Fujimoto, Y. Hori, T. Yamaguchi, and S. Nakagawa, "Proposal of perfect tracking and perfect disturbance rejection control by multirate sampling and applications to hard disk drive control," in *Conf. Decision Contr.*, pp. 5277–5282, 1999.

[7]   Y. Hori, T. Umeno, T. Uchida, and Y. Konno, "An instantaneous speed observer for high performance control of dc servomotor using DSP and low precision shaft encoder," in *4th European Conf. on Power Electronics*, vol. 3, pp. 647–652, 1991.

[8]   S. Hara, Y. Yamamoto, T. Omata, and M. Nakano, "Repetitive control system – a new-type servo system," *IEEE Trans. Automat. Contr.*, vol. 33, pp. 659–668, 1988.

[9]   H. Fujimoto and Y. Hori, "Vibration suppression and optimal repetitive disturbance rejection control in semi-nyquist frequency region using multirate sampling control," in *Conf. Decision Contr.*, pp. 691–700, 2000.

[10]   C. Kempf, W. Messner, M. Tomizuka, and R. Horowitz, "Comparison of four discrete-time repetitive algorithms," *IEEE Contr. Syst. Mag.*, vol. 13, no. 5, pp. 48–54, 1993.

[11]   H. Fujimoto, A. Kawamura, and M. Tomizuka, "Generalized digital redesign method for linear feedback system based on N-delay control," *IEEE/ASME Trans. Mechatronics*, vol. 4, no. 2, pp. 101–109, 1999.

[12]   M. Araki and T. Hagiwara, "Pole assignment by multirate-data output feedback," *Int. J. Control*, vol. 44, no. 6, pp. 1661–1673, 1986.

[13]   T. Murakami and K. Ohnishi, "A study of stability and workspace decoupling control based on robust control in multi-degrees-of-freedom robot," *Trans. IEE of Japan*, vol. 113-D, no. 5, pp. 639–646, 1993. (in Japanese).

[14]   H. Fujimoto, *General Framework of Multirate Sampling Control and Applications to Motion Control Systems.* PhD thesis, The University of Tokyo, December 2000.